



**HAL**  
open science

## **An intranasal lentiviral booster reinforces the waning mRNA vaccine-induced SARS-CoV-2 immunity that it targets to lung mucosa**

Benjamin Vesin, Jodie Lopez, Amandine Noirat, Pierre Authié, Ingrid Fert, Fabien Le Chevalier, Fanny Moncoq, Kirill Nemirov, Catherine Blanc, Cyril Planchais, et al.

### ► To cite this version:

Benjamin Vesin, Jodie Lopez, Amandine Noirat, Pierre Authié, Ingrid Fert, et al.. An intranasal lentiviral booster reinforces the waning mRNA vaccine-induced SARS-CoV-2 immunity that it targets to lung mucosa. *Molecular Therapy*, 2022, 10.1016/j.ymthe.2022.04.016 . pasteur-03695076

**HAL Id: pasteur-03695076**

**<https://pasteur.hal.science/pasteur-03695076>**

Submitted on 14 Jun 2022

**HAL** is a multi-disciplinary open access archive for the deposit and dissemination of scientific research documents, whether they are published or not. The documents may come from teaching and research institutions in France or abroad, or from public or private research centers.

L'archive ouverte pluridisciplinaire **HAL**, est destinée au dépôt et à la diffusion de documents scientifiques de niveau recherche, publiés ou non, émanant des établissements d'enseignement et de recherche français ou étrangers, des laboratoires publics ou privés.



Distributed under a Creative Commons Attribution - NonCommercial 4.0 International License

1 **An intranasal lentiviral booster reinforces the waning mRNA vaccine-induced SARS-CoV-2**  
2 **immunity that it targets to lung mucosa**

3  
4 Running title: Boosting mRNA-induced SARS-CoV-2 immunity with a lentiviral-based nasal  
5 vaccine

6  
7 Benjamin Vesin<sup>1,£</sup>, Jodie Lopez<sup>1,£</sup>, Amandine Noirat<sup>1,£</sup>, Pierre Authié<sup>1,£</sup>, Ingrid Fert<sup>1</sup>, Fabien Le  
8 Chevalier<sup>1</sup>, Fanny Moncoq<sup>1</sup>, Kirill Nemirov<sup>1</sup>, Catherine Blanc<sup>1</sup>, Cyril Planchais<sup>2</sup>, Hugo Mouquet<sup>2</sup>,  
9 Françoise Guinet<sup>3</sup>, David Hardy<sup>4</sup>, Francina Langa Vives<sup>5</sup>, Christiane Gerke<sup>6</sup>, François Anna<sup>1</sup>,  
10 Maryline Bourguin<sup>1</sup>, Laleh Majlessi<sup>1,\$,\*</sup>, ✉, and Pierre Charneau<sup>1,\$,\*</sup>

11  
12 <sup>1</sup> Pasteur-TheraVectys Joint Lab, Institut Pasteur, Virology Department, 28 rue du Dr. Roux,  
13 Paris F-75015, France

14 <sup>2</sup> Laboratory of Humoral Immunology, Université de Paris, Immunology Department, Institut  
15 Pasteur, INSERM U1222, Paris F-75015, France

16 <sup>3</sup> Lymphocytes and Immunity Unit, Université de Paris, Immunology Department, Institut  
17 Pasteur, Paris F-75015, France

18 <sup>4</sup> Histopathology platform, Institut Pasteur, Paris F-75015, France

19 <sup>5</sup> Mouse Genetics Engineering, Institut Pasteur, Paris F-75015, France

20 <sup>6</sup> Institut Pasteur, Université de Paris, Innovation Office, Vaccine Programs, Institut Pasteur,  
21 Paris F-75015, France

22

23

24 <sup>£</sup>These authors contributed equally

25 <sup>\$</sup>Senior authors

26 ✉ Corresponding author: [laleh.majlessi@pasteur.fr](mailto:laleh.majlessi@pasteur.fr)

27

28 **Keywords**

29 Intranasal Vaccination / Lentiviral Vaccine / SARS-CoV-2 Emerging Variants of Concern /  
30 Mucosal Immunity / Mucosal Booster Vaccine / Waning anti-COVID-19 Immunity

31        **Abstract**

32        As the COVID-19 pandemic continues and new SARS-CoV-2 variants of concern emerge, the  
33        adaptive immunity initially induced by the first-generation COVID-19 vaccines starts waning and  
34        needs to be strengthened and broadened in specificity. Vaccination by the nasal route induces  
35        mucosal, humoral and cellular immunity at the entry point of SARS-CoV-2 into the host organism  
36        and has been shown to be the most effective for reducing viral transmission. The lentiviral  
37        vaccination vector (LV) is particularly suitable for this route of immunization due to its non-  
38        cytopathic, non-replicative and scarcely inflammatory properties. Here, to set up an optimized  
39        cross-protective intranasal booster against COVID-19, we generated an LV encoding stabilized  
40        Spike of SARS-CoV-2 Beta variant (LV::S<sub>Beta-2P</sub>). mRNA vaccine-primed and -boosted mice, with  
41        waning primary humoral immunity at 4 months post-vaccination, were boosted intranasally with  
42        LV::S<sub>Beta-2P</sub>. Strong boost effect was detected on cross-sero-neutralizing activity and systemic T-cell  
43        immunity. In addition, mucosal anti-Spike IgG and IgA, lung resident B cells, and effector memory  
44        and resident T cells were efficiently induced, correlating with complete pulmonary protection  
45        against the SARS-CoV-2 Delta variant, demonstrating the suitability of the LV::S<sub>Beta-2P</sub> vaccine  
46        candidate as an intranasal booster against COVID-19. LV::S<sub>Beta-2P</sub> vaccination was also fully  
47        protective against Omicron infection of the lungs and central nervous system, in the highly  
48        susceptible B6.K18-hACE2<sup>IP-THV</sup> transgenic mice.

## 49      **Introduction**

50      Considering: (i) the sustained pandemicity of coronavirus disease 2019 (COVID-19), (ii)  
51      weakening protection potential of the first-generation vaccines against Severe Acute Respiratory  
52      Syndrome beta-coronavirus 2 (SARS-CoV-2), and (iii) the ceaseless emergence of new viral  
53      Variants of Concerns (VOCs), new effective vaccine platforms can be critical for future primary or  
54      booster vaccines <sup>1</sup>. We recently demonstrated the strong performance of a non-integrative lentiviral  
55      vaccination vector (LV) encoding the full-length sequence of Spike glycoprotein (S) from the  
56      ancestral SARS-CoV-2 (LV::S), when used in systemic prime followed by intranasal (i.n.) boost in  
57      multiple preclinical models <sup>2</sup>. LV::S ensures complete (cross) protection of the respiratory tract  
58      against ancestral SARS-CoV-2 and VOCs <sup>3</sup>. In addition, in our new transgenic mice expressing  
59      human Angiotensin Converting Enzyme 2 (hACE2) and displaying unprecedented permissiveness  
60      of the brain to SARS-CoV-2 replication, an i.n. boost with LV::S is required for full protection of  
61      the central nervous system <sup>3</sup>. LV::S is intended to be used as a booster for individuals who already  
62      have been vaccinated against and/or infected by SARS-CoV-2, to reinforce and broaden protection  
63      against emerging VOCs with immune evasion potential <sup>4</sup>.

64      Vaccine LVs are non-integrating, non-replicative, non-cytopathic and negligibly inflammatory  
65      <sup>5,6</sup>. These vectors are pseudotyped with the heterologous glycoprotein from Vesicular Stomatitis  
66      Virus (VSV-G) which confers them a broad tropism for various cell types, including dendritic cells.  
67      The latter are mainly non-dividing cells and thus usually hardly permissive to gene transfer.  
68      However, LVs possess the crucial ability to efficiently transfer genes to the nuclei of not only  
69      dividing but also non-dividing cells, therefore making efficient transduction of non-dividing  
70      immature dendritic cells possible. The resulting endogenous antigen expression in dendritic cells,  
71      with their unique ability to activate naïve T cells <sup>7</sup>, correlates with a strong induction of high-quality  
72      effector and memory T cells <sup>8</sup>. Importantly, the VSV-G pseudo-typing of LVs prevents them from  
73      being targets of preexisting vector-specific immunity in humans, which is key in vaccine  
74      development <sup>5,6</sup>. The safety of LVs has been established in humans in a phase I/IIa Human  
75      Immunodeficiency Virus-1 therapeutic vaccine trial, although the LV used in that clinical trial had  
76      been an integrative version <sup>10,11</sup>. Because of their non-cytopathic and non-inflammatory properties  
77      <sup>10,11</sup>, LVs are well suited for mucosal vaccination. The i.n. immunization approach is expected to  
78      trigger mucosal IgA responses, as well as resident B and T lymphocytes in the respiratory tract <sup>12</sup>.  
79      This immunization route has also been shown to be the most effective at reducing SARS-CoV-2  
80      transmission in both hamster and macaque preclinical models <sup>13</sup>. Induction of mucosal immunity by  
81      i.n. immunization allows SARS-CoV-2 neutralization, directly at the gateway to the host organism,  
82      before it gains access to major infectable anatomical sites <sup>2</sup>.

83 The duration of the protection conferred by the first generation COVID-19 vaccines is not yet  
84 well established, hardly predictable with serological laboratory tests, inconsistent among  
85 individuals and against distinct VOCs. Despite high vaccination rates, the current exacerbation of  
86 the world-wide pandemic indicates that repeated booster immunizations will be needed to ensure  
87 individual and collective immunity against COVID-19. In this context, the safety and potential  
88 adverse effects of multiple additional homologous doses of the first generation COVID-19 vaccines,  
89 for instance related to allergic reaction to polyethylene glycol (PEG) contained in mRNA vaccines,  
90 have to be considered <sup>14</sup>. Importantly, a heterologous prime-boost vaccine delivery method has been  
91 proven to be a more successful strategy than the homologous prime-boost approach in numerous  
92 preclinical models of various infectious diseases <sup>15-17</sup>. Therefore, new efficient vaccination  
93 platforms are of particular interest to develop heterologous boosters against COVID-19. The LV::S  
94 vaccine candidate has potential for prophylactic use against COVID-19, mainly based on its  
95 powerful capacity to induce not only strong neutralizing humoral responses, but also and most  
96 importantly, robust protective T-cell responses which preserve their immune detection of spike  
97 from SARS-CoV-2 VOCs, despite the accumulation of escape mutations <sup>3</sup>. The basis for the  
98 immunogenicity of LVs is usually the genetic message they deliver to host cells and that encodes  
99 the targeted antigen. However, in the particular case of viral envelope proteins used as antigens, that  
100 comprise the transmembrane and the tail segments, it cannot be excluded that the LV is  
101 pseudotyped by both VSV-G and the viral envelope protein they encode. In the context of LV::SFL,  
102 the possible Spike glycoprotein on the LV surface may contribute to the induction of immune  
103 responses, in addition to the genetic message which is translated and expressed by the antigen  
104 presenting cells. LV::S is remarkably suited to be used, as a heterologous i.n. booster vaccine, to  
105 reinforce and broaden protection against the emerging VOCs, while collective immunity in early  
106 vaccinated nations is waning a few months after completion of the initial immunizations, and while  
107 new waves of infections are on the rise <sup>4</sup>.

108 In the present study, toward the preparation of a clinical trial, we first generated an LV encoding  
109 the down-selected S<sub>CoV-2</sub> of the Beta variant, stabilized by K<sup>986</sup>P and V<sup>987</sup>P substitutions in the S2  
110 domain of S<sub>CoV-2</sub> (LV::S<sub>Beta-2P</sub>). In mice, primed and boosted intramuscularly (i.m.) with mRNA  
111 vaccine encoding for the ancestral S<sub>CoV-2</sub> <sup>18,19</sup> and in which the (cross) sero-neutralization potential  
112 was progressively decreasing, we investigated the systemic and mucosal immune responses and the  
113 protective potential of an i.n. LV::S<sub>Beta-2P</sub> heterologous boost.

## 114 **Results**

### 115 **Antigen design and down-selection of a lead candidate**

116 To select the most suitable  $S_{CoV-2}$  variant to induce the greatest neutralization breadth based on  
117 the known variants, we generated LVs encoding the full length  $S_{CoV-2}$  from the Alpha, Beta or  
118 Gamma SARS-CoV-2 VOCs. C57BL/6 mice ( $n = 5/\text{group}$ ) were primed i.m. (wk 0) and boosted  
119 i.m. (wk 3) with  $1 \times 10^8$  TU/mouse of each individual LV and the (cross) neutralization potential  
120 of their sera was assessed before boost (wk 3) and after boost (wk 5) against pseudoviruses  
121 carrying various  $S_{CoV-2}$  (**Figure 1A**). These pseudo-viruses are LV particles that carry the Spike of  
122 interest on their surface but do not have the genetic message for Spike and should not be confused  
123 with the LV-based vaccine that carries the genetic message encoding Spike. Immunization with  
124 LV:: $S_{Alpha}$  generated appropriate neutralization capacity against  $S_{D614G}$  and  $S_{Alpha}$  but not against  
125  $S_{Beta}$  and  $S_{Gamma}$  (**Figure 1B**). Between LV:: $S_{Beta}$  and LV:: $S_{Gamma}$ , the former generated the highest  
126 cross sero-neutralization potential against  $S_{D614G}$ ,  $S_{Alpha}$  and  $S_{Gamma}$  variants. In accordance with  
127 previous observations using other vaccination strategies, in the context of immunization with LV,  
128 the  $K^{986}P - V^{987}P$  substitutions in the S2 domain of  $S_{CoV-2}$  improved the (cross) sero-neutralization  
129 potential (**Figure 1C**), probably due to an extended half-life of  $S_{CoV-2-2P}$ <sup>20</sup>.

130 Taken together these data allowed to down select  $S_{Beta-2P}$  as the best cross-reactive antigen  
131 candidate to be used in the context of LV (LV:: $S_{Beta-2P}$ ) to strengthen the waning immunity  
132 previously induced by the first generation COVID-19 vaccines, like mRNA. Although, the  
133 comparison between WT and 2P forms was performed here with the D614G sequence,  
134 stabilization by the 2P substitution is so well documented<sup>20</sup> that an extrapolation to  $S_{Beta}$  seemed  
135 well founded.

### 136 **Follow-up of humoral immunity in mRNA-primed and -boosted mice and effect of** 137 **LV:: $S_{Beta-2P}$ i.n. boost**

138 We analyzed the potential of LV:: $S_{Beta-2P}$  i.n. boost vaccination to strengthen and broaden the  
139 immune responses in mice which were initially primed and boosted with mRNA and in which the  
140 (cross) sero-neutralization potential was decreasing. C57BL/6 mice were primed i.m. at wk 0 and  
141 boosted i.m. at wk 3 with 1  $\mu\text{g}/\text{mouse}$  of mRNA (**Figure 2A**). In mRNA-primed mice, serum anti-  
142  $S_{CoV-2}$  and anti-RBD IgG were detected at wk 3, increased after mRNA boost as studied at wk 6  
143 and 10, and then decreased at wk 17 in the absence of an additional boost (**Figure S1A**).

144 Longitudinal serological follow-up demonstrated that at 3 wks post prime, cross-neutralization  
145 activities against both  $S_{D614G}$  and  $S_{Alpha}$  were readily detectable (**Figure 2B**). Cross sero-  
146 neutralization was also detectable, although to a lesser degree, against  $S_{Gamma}$ , but not against

147  $S_{\text{Beta}}$ ,  $S_{\text{Delta}}$  or  $S_{\text{Delta+}}$ . At wk 6, i.e., 3 wks post boost, cross sero-neutralization activities against all  
148  $S_{\text{CoV-2}}$  variants were detectable, although at significantly lesser extents against  $S_{\text{Beta}}$ ,  $S_{\text{Delta}}$  and  
149  $S_{\text{Delta+}}$ . From wk 6 to wk 10, cross sero-neutralization against  $S_{\text{Beta}}$ ,  $S_{\text{Delta}}$ , or  $S_{\text{Delta+}}$  gradually and  
150 significantly decreased. At wk 10, half of the mice lost the cross sero-neutralization potential  
151 against  $S_{\text{Beta}}$ ,  $S_{\text{Delta}}$ , or  $S_{\text{Delta+}}$  (Figure 2B).

152 At wk 15, groups of mRNA-primed and -boosted mice were injected i.m. with 1  $\mu\text{g}$  of mRNA  
153 vaccine or PBS. The dose of 1  $\mu\text{g}$  of mRNA per mouse has been demonstrated to be fully  
154 protective in mice<sup>21</sup>. In parallel, at this time point, mRNA-primed and -boosted mice received i.n.  
155  $1 \times 10^9$  Transduction Units (TU)/mouse of an empty LV (LV Ctrl) or escalating doses of  $1 \times 10^6$ ,  
156  $1 \times 10^7$ ,  $1 \times 10^8$ , or  $1 \times 10^9$  TU of LV:: $S_{\text{Beta-2P}}$  (Figure 2A). Unprimed, age-matched mice received  
157 i.n.  $1 \times 10^9$  TU of LV:: $S_{\text{Beta-2P}}$  or PBS.

158 In the previously mRNA-primed and -boosted mice, injected at wk 15 with a third dose of  
159 mRNA or with  $1 \times 10^8$  or  $1 \times 10^9$  TU of LV:: $S_{\text{Beta-2P}}$ , marked anti- $S_{\text{CoV-2}}$  IgG titer increases were  
160 observed (Figure 2C). The titers of anti- $S_{\text{CoV-2}}$  IgA were higher in the mice injected with  $1 \times 10^9$   
161 TU of LV:: $S_{\text{Beta-2P}}$  than those injected with a third 1  $\mu\text{g}$  dose of mRNA vaccine (Figure 2C). In  
162 agreement with these results, (cross) sero-neutralization activity increased in a dose-dependent  
163 manner with LV:: $S_{\text{Beta-2P}}$  i.n. boost given at wk 15, as studied at wk 17 (Figure 2D). Of note, cross  
164 sero-neutralization activity against  $S_{\text{Omicron}}$ -carrying pseudo-viruses was very low in mRNA-  
165 primed and -boosted mice injected at week 15 with a third dose of mRNA via i.m. or with  $1 \times 10^8$   
166 TU of LV:: $S_{\text{Beta-2P}}$  via i.n.. At the mucosal level, at this time point, titers of anti- $S_{\text{CoV-2}}$  and anti-  
167 RBD IgG in the total lung extracts increased in a dose-dependent manner in LV:: $S_{\text{Beta-2P}}$ -boosted  
168 mice, and the titer obtained with the highest dose of LV:: $S_{\text{Beta-2P}}$  was comparable to that after the  
169 third 1  $\mu\text{g}$  i.m. dose of mRNA vaccine (Figure S1B). Importantly, significant titers of lung anti-  
170  $S_{\text{CoV-2}}$  IgA were only detected in LV:: $S_{\text{Beta-2P}}$ -boosted mice (Figure S1B).

171 At the lung cellular level, CD19<sup>+</sup> B cells which are class-switched and thus surface IgM/IgD<sup>-</sup>  
172 plasma cells, and which express CD38, CD62L, CD73 and CD80, can be defined as lung resident  
173 B cells (Brm)<sup>22,23</sup> (Figure 3A). The proportion of these B cells increased in a dose-dependent  
174 manner in the lungs of mice boosted i.n. with LV:: $S_{\text{Beta-2P}}$  (Figure 3B). Mucosal anti- $S_{\text{CoV-2}}$  IgA  
175 and Brm were barely detectable in the mice boosted i.m. at wk15 with 1  $\mu\text{g}$  of mRNA, which was  
176 the single dose of RNA tested in our experiment and thus serves only as indication.

177 **Systemic and mucosal T-cell immunity after i.n. LV:: $S_{\text{Beta-2P}}$  boost in previously mRNA-**  
178 **primed and -boosted mice**

179 Mice were primed and boosted with 1  $\mu$ g mRNA-vaccine and then boosted i.n. at wk15 with  
180 escalating doses of LV::S<sub>Beta-2P</sub>, according to the above-mentioned regimen (Figure 2A). At wk  
181 17, i.e., two wks after the late boost, systemic anti-S<sub>CoV-2</sub> T-cell immunity was assessed by IFN- $\gamma$ -  
182 specific ELISPOT in the spleen of individual mice after in vitro stimulation with individual S:256-  
183 275, S:536-550 or S:576-590 peptide, encompassing immunodominant S<sub>CoV-2</sub> regions for CD8<sup>+</sup> T  
184 cells in H-2<sup>b</sup> mice<sup>2</sup>. Importantly, the weak anti-S CD8<sup>+</sup> T-cell immunity, detectable in the spleens  
185 of mRNA-primed-boosted mice at wk 17, largely increased following i.n. boost with 1  $\times$  10<sup>8</sup> and 1  
186  $\times$  10<sup>9</sup> TU of LV::S<sub>Beta-2P</sub>, similarly to the increase after i.m. mRNA boost (Figure 4).

187 In parallel, in the same animals, the mucosal anti-S<sub>CoV-2</sub> T-cell immunity was assessed by  
188 intracellular Tc1 and Tc2 cytokine staining in T cell-enriched fractions from individual mice after  
189 in vitro stimulation with autologous bone-marrow-dendritic cells loaded with a pool of S:256-275,  
190 S:536-550 and S:576-590 peptides (Figure 5). In previously mRNA-primed and -boosted mice,  
191 only a few S<sub>CoV-2</sub>-specific IFN- $\gamma$ /TNF/IL-2 CD8<sup>+</sup> T-cell responses were detected in the lungs  
192 (Figure 5). However, the i.n. administration of LV::S<sub>Beta-2P</sub> boosted, these Tc1 responses in a dose  
193 dependent manner. Sizable percentages of these Tc1 cells were induced with 1  $\times$  10<sup>8</sup> or 1  $\times$  10<sup>9</sup> TU  
194 of LV::S<sub>Beta-2P</sub>. mRNA (1  $\mu$ g) i.m. administration had a substantially lower boost effect on  
195 mucosal T cells (Figure 5). Tc2 responses (IL-4, IL-5, IL-10 and IL-13) were not detected in any  
196 experimental group (Figure S2), as assessed in the same lung T-cell cultures.

197 Mucosal lung resident memory T cells (Trm), CD8<sup>+</sup> CD44<sup>+</sup> CD69<sup>+</sup> CD103<sup>+</sup> which are one of  
198 the best correlates of protection in infectious diseases<sup>24</sup>, were readily detected in the mice boosted  
199 i.n. with 1  $\times$  10<sup>8</sup> or 1  $\times$  10<sup>9</sup> TU of LV::S<sub>Beta-2P</sub> (Figure 6A, B). No Trm were detected in the lungs  
200 of mice boosted late with 1  $\mu$ g mRNA i.m..

### 201 **Features of lungs after LV::S<sub>Beta-2P</sub> i.n. administration**

202 To identify the immune cell subsets transduced in vivo by LV after i.n. administration,  
203 C57BL/6 mice were immunized i.n. with the high dose of 1  $\times$  10<sup>9</sup> TU of LV::GFP or LV::nano-  
204 Luciferase (LV::nLuc) as a negative control. Lungs were collected at 4 days post-immunization  
205 and analyzed by cytometry in individual mice. CD45<sup>-</sup> cell subset was devoid of GFP<sup>+</sup> cells. Only  
206 very few GFP<sup>+</sup> cells were detected in the CD45<sup>+</sup> hematopoietic cells (Figure S3A-C). The CD45<sup>+</sup>  
207 GFP<sup>+</sup> cells were located in a CD11b<sup>hi</sup> subset and in the CD11b<sup>int</sup> CD11c<sup>+</sup> CD103<sup>+</sup> MHC-II<sup>+</sup>  
208 (dendritic cells) (Figure S3B).

209 To evaluate possible lung infiltration after LV i.n. administration, C57BL/6 mice were injected  
210 i.n. with the high dose of 1  $\times$  10<sup>9</sup> TU of LV::S<sub>Beta-2P</sub> or PBS as a negative control. Lungs were  
211 collected at 1, 3 or 14 days post-injection for histopathological analysis. H&E histological sections

212 displayed minimal to moderate inflammation, interstitial and alveolar syndromes in both  
213 experimental groups, regardless of the three time points investigated. No specific immune  
214 infiltration or syndrome was detected in the animals treated i.n. with  $1 \times 10^9$  TU of LV::S<sub>Beta-2P</sub>,  
215 compared to PBS (**Figure S4A, B**).

#### 216 **Protection of lungs in mRNA-primed and -boosted mice, and later boosted i.n. with** 217 **LV::S<sub>Beta-2P</sub>**

218 We then evaluated the protective vaccine efficacy of LV::S<sub>Beta-2P</sub> i.n. in mRNA-primed and -  
219 boosted mice. At wk 15, mRNA-primed and -boosted mice received i.m. 1 µg of mRNA or PBS. In  
220 parallel, mRNA-primed and -boosted mice received i.n.  $1 \times 10^8$  TU of LV::S<sub>Beta-2P</sub> or control empty  
221 LV. (**Figure 7A**). The choice of this dose was based on our previous experience in which this dose  
222 was fully effective in protection in homologous LV::S prime-boost regimens<sup>2,3</sup>, even though it does  
223 not result in the strongest immune responses. Unvaccinated, age- and sex-matched controls were left  
224 unimmunized. Five weeks after the late boost, i.e. at wk 20, all mice were pre-treated with  $3 \times 10^8$   
225 Infectious Genome Units (IGU) of an adenoviral vector serotype 5 encoding hACE2 (Ad5::hACE2)  
226 <sup>2</sup> to render their lungs permissive to SARS-CoV-2 replication (**Figure 7A**). Four days later, mice  
227 were challenged with SARS-CoV-2 Delta variant, which at the time of this study, i.e. November  
228 2021, was the dominant SARS-CoV-2 variant worldwide.

229 At day 3 post infection, primary analysis of the total lung RNA showed that hACE2 mRNA was  
230 similarly expressed in all mice after Ad5::hACE2 *in vivo* transduction (**Figure 7B**). Lung viral  
231 loads were then determined at 3 dpi by assessing total E RNA and sub-genomic (Esg) E<sub>CoV-2</sub> RNA  
232 qRT-PCR, the latter being an indicator of active viral replication<sup>25-27</sup>. In mice initially primed and  
233 boosted with mRNA-vaccine and then injected i.n. with the control LV or i.m. with PBS, no  
234 significant protective capacity was detectable (**Figure 7C**). In contrast, the LV::S<sub>Beta-2P</sub> i.n. boost of  
235 the initially mRNA vaccinated mice drastically reduced the total E RNA content of SARS-CoV-2  
236 and no copies of the replication-related Esg E<sub>CoV-2</sub> RNA were detected in this group (**Figure 7C**). In  
237 the group which received a late mRNA i.m. boost, the total E RNA content was also significantly  
238 reduced and the content of Esg E<sub>CoV-2</sub> RNA was undetectable in 3 out of 5 in this group.

239 Therefore, a late LV::S<sub>Beta-2P</sub> heterologous i.n. boost, given at wk 15 after the first injection of  
240 mRNA, at the dose of  $1 \times 10^8$  TU/mouse resulted in complete protection, i.e. total absence of viral  
241 replication in 100% of animals, against a high dose challenge with SARS-CoV-2 Delta variant.

#### 242 **Full cross-protective capacity of LV::S<sub>Beta-2P</sub> against SARS-CoV-2 Omicron BA.1 variant**

243 Given the timing of the lengthy preparation of mRNA-primed and -boosted mice, again  
244 boosted i.n. with LV::S<sub>Beta-2P</sub> at wk 15 (July-November 2021), and the emergence of the Omicron

245 variant (December 2021), it was not possible for us to evaluate the anti-Omicron cross-protection  
246 potential of LV::S<sub>Beta-2P</sub> used as a late i.n. boost in parallel. However, we evaluated the protective  
247 efficacy of LV::S<sub>Beta-2P</sub> in the very sensitive B6.K18-hACE2<sup>IP-THV</sup> transgenic mice, which are  
248 prone to SARS-CoV-2 infection in the lung, and in addition display unprecedented brain  
249 permissiveness to SARS-CoV-2 replication <sup>3</sup>. B6.K18-hACE2<sup>IP-THV</sup> mice ( $n = 5-8/\text{group}$ ) were  
250 primed i.m. with  $1 \times 10^8$  TU/mouse of LV::S<sub>Beta-2P</sub> or an empty LV at wk 0 and then boosted i.n. at  
251 wk 3 with the same dose of the same vectors (**Figure 8A**). Mice were then challenged (i.n.) with  
252  $0.3 \times 10^5$  TCID<sub>50</sub> of a SARS-CoV-2 Omicron BA.1 variant <sup>28</sup> at wk 5. Lung and brain viral RNA  
253 contents were then determined at day 5 post infection by using Esg E<sub>CoV-2</sub> RNA qRT-PCR.  
254 LV::S<sub>Beta-2P</sub> vaccination conferred sterilizing protection against SARS-CoV-2 Omicron in the  
255 lungs and brain *versus* high rates of viral replication in the sham-vaccinated controls (**Figure 8B**).  
256 Of note, even if 2 mice out of 8 did not show cervical infection with Omicron, the six others  
257 showed significant replication in the brain.

258 Therefore the LV::S<sub>Beta-2P</sub> displays a full cross-protective capacity against the Omicron variant,  
259 which is fully comparable to its efficiency against the ancestral <sup>2,3</sup> or the Delta variant.

260

261 **Discussion**

262 With the weakly persistent prophylactic potential of the immunity initially induced by the first-  
263 generation COVID-19 vaccines, especially against new VOCs, administration of additional vaccine  
264 doses becomes essential <sup>1</sup>. As an alternative to additional doses of the same vaccines, combining  
265 vaccine platforms in a heterologous prime-boost regimen holds promise for gaining protective  
266 efficacy <sup>29</sup>. Compared to homologous vaccine dose administrations, heterologous prime-boost  
267 strategies may reinforce more efficiently specific adaptive immune responses and long-term  
268 protection <sup>30</sup>. Furthermore, the sequence of the Spike antigen has to be adapted according to the  
269 dynamics of SARS-CoV-2 VOC emergence in order to induce the greatest neutralization breadth.  
270 Protection against symptomatic SARS-CoV-2 infection is mainly related to sero-neutralizing  
271 activity, while CD8<sup>+</sup> T-cell immunity, with their ability to cytolysis virus-infected cells, especially  
272 control the virus replication and result in resolution of viral infection <sup>31</sup>. Therefore, an appropriate  
273 B- and T-cell vaccine platform, including an adapted S<sub>CoV2</sub> sequence, is of utmost interest at the  
274 current step of the pandemic.

275 The LV-based strategy, is highly efficient, not only in inducing humoral responses but also, and  
276 particularly, in establishing high quality and memory T-cell responses <sup>8</sup>. This makes it a suitable  
277 platform for a heterologous boost, even if it is also largely efficacious on its own as a primary  
278 COVID-19 vaccine candidate <sup>2,3</sup>. Furthermore, LVs are non-cytopathic, non-replicative and  
279 scarcely inflammatory. They can thus be used to perform non-invasive i.n. boost to efficiently  
280 induce sterilizing mucosal immunity, which protects the respiratory system as well as the central  
281 nervous system <sup>2,3</sup>. The i.n. route of vaccination has been shown by several teams to be the best at  
282 reducing viral contents in nasal swabs and nasal olfactory neuroepithelium <sup>32,33</sup>, which can  
283 contribute to blocking the respiratory chain of SARS-CoV-2 transmission. One of the advantages of  
284 LV-based immunization is the induction of strong T-cell immune responses with high cross-  
285 reactivity of T-cell epitopes from Spike of diverse VOCs. Therefore, when the neutralizing  
286 antibodies fail or wane, the T-cell arm of the response remains largely protective, as we recently  
287 described in antibody-deficient, B-cell compromised  $\mu$ MT KO mice <sup>3</sup>. This property is relative to a  
288 high-quality and long-lasting T-cell immunity induced against multiple preserved T-cell epitopes,  
289 despite the mutations accumulated in the Spike of the emerging VOCs <sup>3</sup>, including the Omicron  
290 variant.

291 In the present study, we down-selected the S<sub>Beta-2P</sub> antigen which induced the greatest  
292 neutralization breadth against the main SARS-CoV-2 VOCs and designed a non-integrative LV  
293 encoding a stabilized version of this antigen. The induction of highly cross-reactive neutralizing  
294 antibodies by SARS-CoV-2 Beta variant has been well documented <sup>34</sup>. The notable ability of S<sub>Beta</sub>

295 to elicit cross-reactive antibodies correlates with: (i) the shared genetic and structural features of  
296 these antibodies, (ii) their preferential use of specific germline sequences, such as VH1-58 and  
297 VH4-39, and (iii) their relatively low number of somatic hypermutations. Collectively, it seems that  
298 there exists some common paratopes in such S<sub>Beta</sub>-elicited cross-reactive antibodies which interact  
299 with the Y501 mutation found in RBD of Alpha, Beta, and Gamma<sup>35</sup>.

300 In mice primed and boosted with mRNA vaccine (encoding the ancestral S<sub>CoV-2</sub> sequence), with  
301 waning (cross) sero-neutralization capabilities, we used escalating doses of LV::S<sub>Beta-2P</sub> for an i.n.  
302 late boost. We demonstrated a dose-dependent increase in anti-S<sub>CoV-2</sub> IgG and IgA titers, and a  
303 broadened sero-neutralization potential both in the sera and lung homogenates against VOCs. No  
304 anti-S<sub>CoV-2</sub> IgA was detected in the lungs of mice injected with the third dose of 1 µg of mRNA  
305 given via i.m. injection. Increasing proportions of non-circulating Brm, defined as class-switched  
306 surface IgM<sup>-</sup>/IgD<sup>-</sup> plasma cells, with CD38<sup>+</sup> CD73<sup>+</sup> CD62L<sup>+</sup> CD69<sup>+</sup> CD80<sup>+</sup> phenotype<sup>22,23</sup>, were  
307 detected in a dose-dependent manner, in the lungs of mice boosted i.n. with LV::S<sub>Beta-2P</sub>.

308 Spike-specific, effector lung CD8<sup>+</sup> Tc1 cells were largely detected in the initially mRNA-  
309 primed and boosted mice which received a late i.n. LV::S<sub>Beta-2P</sub> boost. These lung CD8<sup>+</sup> T cells did  
310 not display Tc2 phenotype. Increasing proportions of lung CD8<sup>+</sup> CD44<sup>+</sup> CD69<sup>+</sup> CD103<sup>+</sup> Trm were  
311 also detected, in a dose-dependent manner, only in LV::S<sub>Beta-2P</sub> i.n. boosted mice. The systemic  
312 CD8<sup>+</sup> T-cell responses against various immunogenic regions of S<sub>CoV-2</sub> were also increased with 1  
313 × 10<sup>8</sup> or 1 × 10<sup>9</sup> TU doses of LV::S<sub>Beta-2P</sub> i.n. boost in the initially mRNA-primed and -boosted  
314 mice. The highest i.n. dose of LV::S<sub>Beta-2P</sub> was comparable to the third injection of 1 µg/mouse  
315 of mRNA given by i.m. injection. The fact that the i.n. administration of LV::S<sub>Beta-2P</sub> had a  
316 substantial boost effect on the systemic T-cell immunity indicates that this boost pathway is not at  
317 the expense of the induction of systemic immunity. As we recently determined by epitope  
318 mapping and cytometric analysis, LV::S immunization only induced CD8<sup>+</sup> - but not CD4<sup>+</sup> - T  
319 cells against S<sub>CoV-2</sub><sup>2</sup>. This results from direct transduction of antigen-presenting cells by LVs and  
320 thus efficient antigen routing to the MHC-I machinery but not to the endocytic and MHC-II  
321 presentation pathway (our unpublished observation). Furthermore, as LVs are not cytopathic, the  
322 initially transduced antigen-presenting cells should not generate marked amounts of cell debris  
323 that could be taken up by secondary antigen-presenting cells for MHC-II presentation.

324 Evaluation of the protection in mRNA-primed and -boosted mice, showed that 20 wk after the  
325 first injection of mRNA vaccine, there was no protection detectable in the lungs against infection  
326 with the SARS-CoV-2 Delta variant. Importantly, an i.n. boost at wk 15 with the dose of 1 × 10<sup>8</sup>  
327 TU/mouse LV::S<sub>Beta-2P</sub> resulted in full inhibition of SARS-CoV-2 replication in the lungs upon  
328 challenge with the Delta variant at wk 20. In the mice receiving an 1 µg mRNA i.m. boost at wk

329 15 the lung SARS-CoV-2 RNA contents was reduced in a statistically comparable manner, albeit  
330 without total inhibition of viral replication in all mice.

331 The lack of protection against the Delta variant infection only four months after the initial  
332 systemic prime-boost by mRNA vaccine, as we observed in the preclinical model in this study, may  
333 be explained by the weak efficiency of the ancestral  $S_{\text{CoV-2}}$  sequence to induce long-lasting  
334 neutralizing antibodies against the recent VOCs. In addition, it can be hypothesized that the  
335 adaptive immune memory induced by i.m. mRNA immunization is likely to be localized in  
336 secondary lymphoid organs at anatomical sites located far from the upper respiratory tract. In such a  
337 context, the extraordinary rapid replication of new VOCs, such as Delta or Omicron, in the upper  
338 respiratory tract would not leave enough time for the reactivation of immune memory from remote  
339 anatomical sites and the recruitment of the immune arsenal from these sites. In human populations,  
340 such scenario would lead to a high possibility of viral replication and variable levels of its  
341 transmission, which would prevent the epidemic from being completely contained by mass  
342 vaccination through the systemic route.

343 It is not yet known if a single third booster will extend and maintain the protective potential, or  
344 whether semi-regular boosters will be required against COVID-19 in the future. The LV:: $S_{\text{Beta-2P}}$  i.n.  
345 boost strengthens the intensity, broadens the VOC cross-recognition, and targets B-and T-cell  
346 immune responses to the principal entry point of SARS-CoV-2, that is, to the mucosal respiratory  
347 tract of the host organism preventing the infection of main anatomical sites. It is interesting to note  
348 that in rodents only a pair of cervical ganglia exists versus a large network of such ganglia in  
349 humans<sup>36</sup>. Following i.n. immunization, this anatomical feature in humans may provide an even  
350 more consistent site of immune response induction and local memory maintenance, at the vicinity  
351 of to the potential site of airway infection. In addition, nasopharynx-associated lymphoid tissue is a  
352 powerful defense system composed of: (i) organized lymphoid tissue, i.e., tonsils, and (ii) a diffuse  
353 nose-associated lymphoid tissues, where effector and memory B and T lymphocytes are able to  
354 maintain long-lasting immunity<sup>37</sup>. This mucosal immune arsenal deserves to be explored in the  
355 control of SARS-CoV-2 transmission in the current context of the pandemic. A phase I clinical trial  
356 is currently in preparation for the use of i.n. boost by LV:: $S_{\text{Beta-2P}}$  in previously vaccinated humans  
357 or in COVID-19 convalescents. Although LVs cause very little or nearly no inflammation<sup>10,11</sup>, to  
358 ensure that i.n. vaccination with LV:: $S_{\text{Beta-2P}}$  will not result in brain inflammation, we plan to  
359 evaluate the toxicity of the preclinical GMP batch in regulatory preclinical assays. We will pay  
360 particular attention to: (i) biodistribution of LV:: $S_{\text{Beta-2P}}$ , to be assessed by PCR, and (ii)  
361 histopathology in as many organs as possible, including the brain, after i.n. administration of the

362 highest dose planned for the clinical trial and according to kinetics pre-established in non-regulatory  
363 preclinical experiments.

364 We have completed a technology transfer to an industrial partner and are now able to produce  
365 LVs in large quantities for clinical trials that will be starting soon. After successful completion of  
366 phase I trials, we plan to move to fermenter production, which is now possible for LV production in  
367 adherent HEK293-T cells. We have also established the high stability of the LVs if appropriate  
368 conservation buffers are used. Compared to adenoviral vectors, LVs have the advantage of being  
369 only scarcely inflammatory and not being targets of pre-existing immunity in human populations  
370 <sup>6,10</sup>. LVs have a particular tropism for dendritic cells, which generates endogenous antigen  
371 expression in these antigen presenting cells, whereas adenoviral vectors preferentially target  
372 epithelial cells which requires indirect and cross-presentation of antigens. This may be the reason  
373 why LVs are effective at much lower doses compared to adenoviral vectors. The doses of  $1 \times 10^8$  or  
374  $1 \times 10^9$  TU are optimal in mice. However, *Mus musculus* species underestimates the efficacy of  
375 HIV-based LVs because of restriction factors which reduces the transduction efficiency of LVs in  
376 the murine cells. In larger animals such as piglets <sup>38</sup>, horses (our unpublished results) and macaques  
377 <sup>39</sup>, as well as in humans <sup>9</sup>, the same range of LV doses are largely effective for the induction of T-  
378 cell responses and protection versus  $1 \times 10^{13}$  adenoviral active particles for human vaccination <sup>6</sup>.

379

## 380 **Materials and Methods**

### 381 **Mice immunization and SARS-CoV-2 infection**

382 Female C57BL/6JRj mice were purchased from Janvier (Le Genest Saint Isle, France), housed in  
383 individually-ventilated cages under specific pathogen-free conditions at the Institut Pasteur animal  
384 facilities and used at the age of 7 wks. Mice were immunized i.m. with 1 µg/mouse of mRNA-1273  
385 (Moderna) vaccine. The Moderna vaccine was provided by the Institut Pasteur Medical Center.  
386 These were leftover unusable vaccines in thawed vials that were not authorized to be pooled for  
387 human vaccination and would have been destroyed. Thus, the doses used in this study did not  
388 deprive any individual of a vaccine dose during the pandemic. For i.n. injections with LV, mice  
389 were anesthetized by i.p. injection of Ketamine (Imalgene, 80 mg/kg) and Xylazine (Rompun, 5  
390 mg/kg). For protection experiments against SARS-CoV-2, mice were transferred into filtered cages  
391 in isolator. Four days before SARS-CoV-2 inoculation, mice were pretreated with  $3 \times 10^8$  IGU of  
392 Ad5::hACE2 as previously described <sup>2</sup>. Mice were then transferred into a level 3 biosafety cabinet  
393 and inoculated i.n. with  $0.3 \times 10^5$  TCID<sub>50</sub> of the Delta variant of SARS-CoV-2 clinical isolate <sup>40</sup>  
394 contained in 20 µl. B6.K18-hACE2<sup>IP-THV</sup> mice <sup>3</sup> were primed i.m. and boosted i.n. by LV::S<sub>Beta-2P</sub>  
395 and then inoculated with  $0.3 \times 10^5$  TCID<sub>50</sub> of the Omicron BA.1 variant of SARS-CoV-2 clinical  
396 isolate <sup>28</sup>. Mice were then housed in filtered cages in an isolator in BioSafety Level 3 animal  
397 facilities. The organs recovered from the infected animals were manipulated according to the  
398 approved standard procedures of these facilities.

### 399 **Ethical approval of animal experimentation**

400 Experimentation on animals was performed in accordance with the European and French  
401 guidelines (Directive 86/609/CEE and Decree 87-848 of 19 October 1987) subsequent to approval  
402 by the Institut Pasteur Safety, Animal Care and Use Committee, protocol agreement delivered by  
403 local ethical committee (CETEA #DAP20007, CETEA #DAP200058) and Ministry of High  
404 Education and Research APAFIS#24627-2020031117362508 v1, APAFIS#28755-  
405 2020122110238379 v1.

### 406 **Construction and production of vaccinal LV::S<sub>Beta-2P</sub>**

407 First, a codon-optimized sequence of Spike from the Ancestral, D614G, Alpha, Beta or Gamma  
408 VOCs were synthesized and inserted into the pMK-RQ\_S-2019-nCoV\_S501YV2 plasmid. The S  
409 sequence was then extracted by BamHI/XhoI digestion to be ligated into the pFlap lentiviral  
410 plasmid between the BamHI and XhoI restriction sites, located between the native human ieCMV  
411 promoter and the mutated *atg* starting codon of Woodchuck Posttranscriptional Regulatory Element  
412 (WPRES) sequence (**Figure S5**). To introduce the K<sup>986</sup>P-V<sup>987</sup>P “2P” double mutation in S<sub>D614G</sub> or

413  $S_{\text{Beta}}$ , a directed mutagenesis was performed by use of Takara In-Fusion kit on the corresponding  
414 pFlap plasmids. Various pFlap-ieCMV-S-WPREm or pFlap-ieCMV-S<sub>2P</sub>-WPREm plasmids were  
415 amplified and used to produce non-integrative vaccinal LV, as previously described <sup>2,6</sup>. The  
416 envelope plasmid, encodes VSV-G under ieCMV promoter and the packaging plasmid contains  
417 *gag*, *pol*, *tat* and *rev* genes. The integrase resulting from this plasmid carries a missense amino acid  
418 in its catalytic triad, i.e., the D64V mutation, that prevents the integration of viral DNA into the host  
419 chromosome. Without integration, the viral DNA remains in an episomal form, very effective for  
420 gene expression <sup>2,6</sup>.

#### 421 **Analysis of humoral and systemic T-cell immunity**

422 Anti-S<sub>CoV-2</sub> IgG and IgA antibody titers were determined by ELISA by use of recombinant  
423 stabilized S<sub>CoV-2</sub> or RBD fragment for coating. Neutralization potential of clarified and  
424 decomplexed sera or lung homogenates was quantitated by use of lentiviral particles pseudo-  
425 typed with S<sub>CoV-2</sub> from diverse variants, as previously described <sup>2,41</sup>.

426 T-splenocyte responses were quantitated by IFN- $\gamma$  ELISPOT after in vitro stimulation with  
427 S:256-275, S:536-550 or S:576-590 synthetic 15-mer peptides which contain S<sub>CoV-2</sub> MHC-I-  
428 restricted epitopes in H-2<sup>d</sup> mice <sup>2</sup>. Spots were quantified in a CTL Immunospot S6 ultimate-V  
429 Analyser by use of CTL Immunocapture 7.0.8.1 program.

#### 430 **Phenotypic and Functional cytometric analysis of lung immune cells**

431 Enrichment and staining of lung immune cells were performed as detailed previously <sup>2,3</sup> after  
432 treatment with 400 U/ml type IV collagenase and DNase I (Roche) for a 30-minute incubation at  
433 37°C and homogenization by use of GentleMacs (Miltenyi Biotech). Cell suspensions were then  
434 filtered through 100  $\mu\text{m}$ -pore filters, centrifuged at 1200 rpm and enriched on Ficoll gradient after  
435 20 min centrifugation at 3000 rpm at RT, without brakes. The recovered cells were co-cultured with  
436 syngeneic bone-marrow derived dendritic cells loaded with a pool of A, B, C peptides, each at 1  
437  $\mu\text{g}/\text{ml}$  or negative control peptide at x  $\mu\text{g}/\text{ml}$ . The following mixture was used to detect lung Tc1  
438 cells: PerCP-Cy5.5-anti-CD3 (45-0031-82, eBioScience), eF450-anti-CD4 (48-0042-82,  
439 eBioScience) and APC-anti-CD8 (17-0081-82, eBioScience) for surface staining and BV650-anti-  
440 IFN-g (563854, BD), FITC-anti-TNF (554418, BD) and PE-anti-IL-2 (561061, BD) for  
441 intracellular staining. The following mixture was used to detect lung Tc2 cells: PerCP-Cy5.5-anti-  
442 CD3 (45-0031-82, eBioScience), eF450-anti-CD4 (48-0042-82, eBioScience), BV711-anti-CD8  
443 (563046, BD Biosciences), for surface staining and BV605-anti-IL-4 (504125, BioLegend Europe  
444 BV), APC-anti-IL-5 (504306, BioLegend Europe BV), FITC-anti-IL-10 (505006, BioLegend  
445 Europe BV), PE-anti-IL-13 (12-7133-81, eBioScience) for intracellular staining. The intracellular

446 staining was performed by use of the Fix Perm kit (BD), following the manufacturer's protocol.  
447 Dead cells were excluded by use of Near IR Live/Dead (Invitrogen). Staining was performed in the  
448 presence of FcγII/III receptor blocking anti-CD16/CD32 (BD).

449 To identify lung resident memory CD8<sup>+</sup> T-cell subsets, a mixture of PerCP-Vio700-anti-CD3  
450 (130-119-656, Miltenyi Biotec), PECy7-CD4 (552775, BD Biosciences), BV510-anti-CD8  
451 (100752, BioLegend), PE-anti-CD62L (553151, BD Biosciences), APC-anti-CD69 (560689, BD  
452 Biosciences), APC-Cy7-anti-CD44 (560568, BD Biosciences), FITC-anti-CD103 (11-1031-82,  
453 eBiosciences) and yellow Live/Dead (Invitrogen) was used. Lung Brm were studied by surface  
454 staining with a mixture of PerCP Vio700-anti-IgM (130-106-012, Miltenyi), and PerCP Vio700-  
455 anti-IgD (130-103-797, Miltenyi), APC-H7-anti-CD19 (560143, BD Biosciences), PE-anti-CD38  
456 (102708, BioLegend Europe BV), PE-Cy7-anti-CD62L (ab25569, AbCam), BV711-anti-CD69  
457 (740664, BD Biosciences), BV421-anti-CD73 (127217, BioLegend Europe BV), FITC-anti-CD80  
458 (104705, BioLegend Europe BV and yellow Live/Dead (Invitrogen).

459 Cells were incubated with appropriate mixtures for 25 minutes at 4°C, washed in PBS containing  
460 3% FCS and fixed with Paraformaldehyde 4% after an overnight incubation at 4°C. Samples were  
461 acquired in an Attune NxT cytometer (Invitrogen) and data analyzed by FlowJo software (Treestar,  
462 OR, USA).

### 463 **Determination of viral RNA content in the organs**

464 Organs from mice were removed and immediately frozen at -80°C on dry ice. RNA from  
465 circulating SARS-CoV-2 was prepared from lungs as described previously<sup>2</sup>. Lung homogenates  
466 were prepared by thawing and homogenizing in lysing matrix M (MP Biomedical) with 500 µl of  
467 PBS using a MP Biomedical Fastprep 24 Tissue Homogenizer. RNA was extracted from the  
468 supernatants of organ homogenates centrifuged during 10 min at 2000g, using the Qiagen Rneasy  
469 kit. The RNA samples were then used to determine viral RNA content by E-specific qRT-PCR. To  
470 determine viral RNA content by Esg-specific qRT-PCR, total RNA was prepared using lysing  
471 matrix D (MP Biomedical) containing 1 mL of TRIzol reagent (ThermoFisher) and homogenization  
472 at 30 s at 6.0 m/s twice using MP Biomedical Fastprep 24 Tissue Homogenizer. The quality of  
473 RNA samples was assessed by use of a Bioanalyzer 2100 (Agilent Technologies). Viral RNA  
474 contents were quantitated using a NanoDrop Spectrophotometer (Thermo Scientific NanoDrop).  
475 The RNA Integrity Number (RIN) was 7.5-10.0. SARS-CoV-2 E or E sub-genomic mRNA were  
476 quantitated following reverse transcription and real-time quantitative TaqMan® PCR, using  
477 SuperScript™ III Platinum One-Step qRT-PCR System (Invitrogen) and specific primers and  
478 probe (Eurofins), as recently described<sup>3</sup>.

479      **Lung histology**

480      Left lobes from lungs were fixed in formalin and embedded in paraffin. Paraffin sections (5- $\mu$ m  
481 thick) were stained with Hematoxylin and Eosin (H&E). Slides were scanned using the AxioScan  
482 Z1 (Zeiss) system and images were analyzed with the Zen 2.6 software. Histological images were  
483 evaluated according to a score of 0 to 5 (normal, minimal, mild, moderate, marked, severe).

484

- 486 1. [https://cdn.who.int/media/docs/default-source/immunization/sage/covid/global-covid-19-vaccination-strategic-487 vision-for-2022\\_sage-yellow-book.pdf?sfvrsn=4827ec0d\\_5](https://cdn.who.int/media/docs/default-source/immunization/sage/covid/global-covid-19-vaccination-strategic-487 vision-for-2022_sage-yellow-book.pdf?sfvrsn=4827ec0d_5). (2021).
- 488 2. Ku, M.W., Bourguine, M., Authie, P., Lopez, J., Nemirov, K., Moncoq, F., Noirat, A., Vesin, B., Nevo, F., 489 Blanc, C., Souque, P., et al. (2021). Intranasal vaccination with a lentiviral vector protects against SARS-CoV- 490 2 in preclinical animal models. *Cell Host Microbe* 29, 236-249 e236. 10.1016/j.chom.2020.12.010.
- 491 3. Ku, M.W., Authie, P., Bourguine, M., Anna, F., Noirat, A., Moncoq, F., Vesin, B., Nevo, F., Lopez, J., Souque, 492 P., Blanc, C., et al. (2021). Brain cross-protection against SARS-CoV-2 variants by a lentiviral vaccine in new 493 transgenic mice. *EMBO Mol Med*, e14459. 10.15252/emmm.202114459.
- 494 4. Juno, J.A., and Wheatley, A.K. (2021). Boosting immunity to COVID-19 vaccines. *Nat Med* 27, 1874-1875. 495 10.1038/s41591-021-01560-x.
- 496 5. Hu, B., Tai, A., and Wang, P. (2011). Immunization delivered by lentiviral vectors for cancer and infectious 497 diseases. *Immunol Rev* 239, 45-61. 10.1111/j.1600-065X.2010.00967.x.
- 498 6. Ku, M.W., Charneau, P., and Majlessi, L. (2021). Use of lentiviral vectors in vaccination. *Expert Rev* 499 *Vaccines*, 1-16. 10.1080/14760584.2021.1988854.
- 500 7. Guernonprez, P., Gerber-Ferder, Y., Vaivode, K., Bourdely, P., and Helft, J. (2019). Origin and development 501 of classical dendritic cells. *Int Rev Cell Mol Biol* 349, 1-54. 10.1016/bs.ircmb.2019.08.002.
- 502 8. Ku, M.W., Authie, P., Nevo, F., Souque, P., Bourguine, M., Romano, M., Charneau, P., and Majlessi, L. (2021). 503 Lentiviral vector induces high-quality memory T cells via dendritic cells transduction. *Commun Biol* 4, 713. 504 10.1038/s42003-021-02251-6.
- 505 9. TheraVectys-Clinical-Trial (2019). Safety, Tolerability and Immunogenicity Induced by the THV01 Treatment 506 in Patients Infected With HIV-1 Clade B and Treated With Highly Active Antiretroviral Therapy (HAART). 507 <https://www.clinicaltrialsregister.eu/ctr-search/search?query=2011-006260-52> 2011-006260-52.
- 508 10. Cousin, C., Oberkamp, M., Felix, T., Rosenbaum, P., Weil, R., Fabrega, S., Morante, V., Negri, D., Cara, A., 509 Dadaglio, G., and Leclerc, C. (2019). Persistence of Integrase-Deficient Lentiviral Vectors Correlates with the 510 Induction of STING-Independent CD8(+) T Cell Responses. *Cell Rep* 26, 1242-1257 e1247. 511 10.1016/j.celrep.2019.01.025.
- 512 11. Lopez, J., Anna, F., Authié, P., Pawlik, A., Ku, M.W., Blanc, C., Souque, P., Moncoq, F., Noirat, A., Hardy, 513 D., Sougakoff, W., et al. An optimized lentiviral vector induces CD4+ T-cell immunity and predicts a booster 514 vaccine against tuberculosis. Submitted.
- 515 12. Lund, F.E., and Randall, T.D. (2021). Scent of a vaccine. *Science* 373, 397-399. 10.1126/science.abg9857.
- 516 13. van Doremalen, N., Purushotham, J.N., Schulz, J.E., Holbrook, M.G., Bushmaker, T., Carmody, A., Port, J.R., 517 Yinda, C.K., Okumura, A., Saturday, G., Amanat, F., et al. (2021). Intranasal ChAdOx1 nCoV-19/AZD1222 518 vaccination reduces viral shedding after SARS-CoV-2 D614G challenge in preclinical models. *Sci Transl Med* 519 13. 10.1126/scitranslmed.abh0755.
- 520 14. Castells, M.C., and Phillips, E.J. (2021). Maintaining Safety with SARS-CoV-2 Vaccines. *N Engl J Med* 384, 521 643-649. 10.1056/NEJMra2035343.
- 522 15. He, Q., Mao, Q., An, C., Zhang, J., Gao, F., Bian, L., Li, C., Liang, Z., Xu, M., and Wang, J. (2021). 523 Heterologous prime-boost: breaking the protective immune response bottleneck of COVID-19 vaccine 524 candidates. *Emerg Microbes Infect* 10, 629-637. 10.1080/22221751.2021.1902245.
- 525 16. Lu, S. (2009). Heterologous prime-boost vaccination. *Curr Opin Immunol* 21, 346-351. 526 10.1016/j.coi.2009.05.016.
- 527 17. Nordstrom, P., Ballin, M., and Nordstrom, A. (2021). Effectiveness of heterologous ChAdOx1 nCoV-19 and 528 mRNA prime-boost vaccination against symptomatic Covid-19 infection in Sweden: A nationwide cohort 529 study. *Lancet Reg Health Eur*, 100249. 10.1016/j.lanepe.2021.100249.
- 530 18. Jackson, L.A., Anderson, E.J., Roupheal, N.G., Roberts, P.C., Makhene, M., Coler, R.N., McCullough, M.P., 531 Chappell, J.D., Denison, M.R., Stevens, L.J., Pruijssers, A.J., et al. (2020). An mRNA Vaccine against SARS- 532 CoV-2 - Preliminary Report. *N Engl J Med* 383, 1920-1931. 10.1056/NEJMoa2022483.
- 533 19. Wang, F., Kream, R.M., and Stefano, G.B. (2020). An Evidence Based Perspective on mRNA-SARS-CoV-2 534 Vaccine Development. *Med Sci Monit* 26, e924700. 10.12659/MSM.924700.
- 535 20. Walls, A.C., Park, Y.J., Tortorici, M.A., Wall, A., McGuire, A.T., and Veesler, D. (2020). Structure, Function, 536 and Antigenicity of the SARS-CoV-2 Spike Glycoprotein. *Cell* 181, 281-292 e286. 10.1016/j.cell.2020.02.058.
- 537 21. Corbett, K.S., Edwards, D.K., Leist, S.R., Abiona, O.M., Boyoglu-Barnum, S., Gillespie, R.A., Himansu, S., 538 Schafer, A., Ziwawo, C.T., DiPiazza, A.T., Dinnon, K.H., et al. (2020). SARS-CoV-2 mRNA vaccine design 539 enabled by prototype pathogen preparedness. *Nature* 586, 567-571. 10.1038/s41586-020-2622-0.
- 540 22. Barker, K.A., Etesami, N.S., Shenoy, A.T., Arafa, E.I., Lyon de Ana, C., Smith, N.M., Martin, I.M., Goltry, 541 W.N., Barron, A.M., Browning, J.L., Kathuria, H., et al. (2021). Lung-resident memory B cells protect against 542 bacterial pneumonia. *J Clin Invest* 131. 10.1172/JCI141810.
- 543 23. Onodera, T., Takahashi, Y., Yokoi, Y., Ato, M., Kodama, Y., Hachimura, S., Kurosaki, T., and Kobayashi, K. 544 (2012). Memory B cells in the lung participate in protective humoral immune responses to pulmonary 545 influenza virus reinfection. *Proc Natl Acad Sci U S A* 109, 2485-2490. 10.1073/pnas.1115369109.

- 546 24. Masopust, D., and Soerens, A.G. (2019). Tissue-Resident T Cells and Other Resident Leukocytes. *Annu Rev Immunol* 37, 521-546. 10.1146/annurev-immunol-042617-053214.
- 547
- 548 25. Chandrashekar, A., Liu, J., Martinot, A.J., McMahan, K., Mercado, N.B., Peter, L., Tostanoski, L.H., Yu, J., Maliga, Z., Nekorchuk, M., Busman-Sahay, K., et al. (2020). SARS-CoV-2 infection protects against
- 549 rechallenge in rhesus macaques. *Science* 369, 812-817. 10.1126/science.abc4776.
- 550
- 551 26. Tostanoski, L.H., Wegmann, F., Martinot, A.J., Loos, C., McMahan, K., Mercado, N.B., Yu, J., Chan, C.N.,
- 552 Bondoc, S., Starke, C.E., Nekorchuk, M., et al. (2020). Ad26 vaccine protects against SARS-CoV-2 severe
- 553 clinical disease in hamsters. *Nat Med* 26, 1694-1700. 10.1038/s41591-020-1070-6.
- 554 27. Wolfel, R., Corman, V.M., Guggemos, W., Seilmaier, M., Zange, S., Muller, M.A., Niemeyer, D., Jones, T.C.,
- 555 Vollmar, P., Rothe, C., Hoelscher, M., et al. (2020). Virological assessment of hospitalized patients with
- 556 COVID-2019. *Nature* 581, 465-469. 10.1038/s41586-020-2196-x.
- 557 28. Planas, D., Saunders, N., Maes, P., Guivel-Benhassine, F., Planchais, C., Buchrieser, J., Bolland, W.H., Porrot,
- 558 F., Staropoli, I., Lemoine, F., Pere, H., et al. (2022). Considerable escape of SARS-CoV-2 Omicron to
- 559 antibody neutralization. *Nature* 602, 671-675. 10.1038/s41586-021-04389-z.
- 560 29. Barros-Martins, J., Hammerschmidt, S.I., Cossmann, A., Odak, I., Stankov, M.V., Morillas Ramos, G.,
- 561 Dopfer-Jablonka, A., Heidemann, A., Ritter, C., Friedrichsen, M., Schultze-Florey, C., et al. (2021). Immune
- 562 responses against SARS-CoV-2 variants after heterologous and homologous ChAdOx1 nCoV-19/BNT162b2
- 563 vaccination. *Nat Med* 27, 1525-1529. 10.1038/s41591-021-01449-9.
- 564 30. Kardani, K., Bolhassani, A., and Shahbazi, S. (2016). Prime-boost vaccine strategy against viral infections:
- 565 Mechanisms and benefits. *Vaccine* 34, 413-423. 10.1016/j.vaccine.2015.11.062.
- 566 31. Sette, A., and Crotty, S. (2021). Adaptive immunity to SARS-CoV-2 and COVID-19. *Cell* 184, 861-880.
- 567 10.1016/j.cell.2021.01.007.
- 568 32. Bricker, T.L., Darling, T.L., Hassan, A.O., Harastani, H.H., Soung, A., Jiang, X., Dai, Y.N., Zhao, H., Adams,
- 569 L.J., Holtzman, M.J., Bailey, A.L., et al. (2021). A single intranasal or intramuscular immunization with
- 570 chimpanzee adenovirus-vectored SARS-CoV-2 vaccine protects against pneumonia in hamsters. *Cell Rep* 36,
- 571 109400. 10.1016/j.celrep.2021.109400.
- 572 33. Hassan, A.O., Feldmann, F., Zhao, H., Curiel, D.T., Okumura, A., Tang-Huau, T.L., Case, J.B., Meade-White,
- 573 K., Callison, J., Chen, R.E., Lovaglio, J., et al. (2021). A single intranasal dose of chimpanzee adenovirus-
- 574 vectored vaccine protects against SARS-CoV-2 infection in rhesus macaques. *Cell Rep Med* 2, 100230.
- 575 10.1016/j.xcrm.2021.100230.
- 576 34. Moyo-Gwete, T., Madzivhandila, M., Makhado, Z., Ayres, F., Mhlanga, D., Oosthuysen, B., Lambson, B.E.,
- 577 Kgagudi, P., Tegally, H., Iranzadeh, A., Doolabh, D., et al. (2021). Cross-Reactive Neutralizing Antibody
- 578 Responses Elicited by SARS-CoV-2 501Y.V2 (B.1.351). *N Engl J Med* 384, 2161-2163.
- 579 10.1056/NEJMc2104192.
- 580 35. Reincke, S.M., Yuan, M., Kornau, H.C., Corman, V.M., van Hoof, S., Sanchez-Sendin, E., Ramberger, M.,
- 581 Yu, W., Hua, Y., Tien, H., Schmidt, M.L., et al. (2022). SARS-CoV-2 Beta variant infection elicits potent
- 582 lineage-specific and cross-reactive antibodies. *Science* 375, 782-787. 10.1126/science.abm5835.
- 583 36. <https://teachmeanatomy.info/neck/vessels/lymphatics/>.
- 584 37. Porzia, A., Cavaliere, C., Begvarfaj, E., Masieri, S., and Mainiero, F. (2018). Human nasal immune system: a
- 585 special site for immune response establishment. *J Biol Regul Homeost Agents* 32, 3-8.
- 586 38. de Wispelaere, M., Ricklin, M., Souque, P., Frenkiel, M.P., Paulous, S., Garcia-Nicolas, O., Summerfield, A.,
- 587 Charneau, P., and Despres, P. (2015). A Lentiviral Vector Expressing Japanese Encephalitis Virus-like
- 588 Particles Elicits Broad Neutralizing Antibody Response in Pigs. *PLoS Negl Trop Dis* 9, e0004081.
- 589 10.1371/journal.pntd.0004081.
- 590 39. Beignon, A.S., Mollier, K., Liard, C., Coutant, F., Munier, S., Riviere, J., Souque, P., and Charneau, P. (2009).
- 591 Lentiviral vector-based prime/boost vaccination against AIDS: pilot study shows protection against Simian
- 592 immunodeficiency virus SIVmac251 challenge in macaques. *J Virol* 83, 10963-10974. 10.1128/JVI.01284-09.
- 593 40. Planas, D., Veyer, D., Baidaliuk, A., Staropoli, I., Guivel-Benhassine, F., Rajah, M.M., Planchais, C., Porrot,
- 594 F., Robillard, N., Puech, J., Prot, M., et al. (2021). Reduced sensitivity of SARS-CoV-2 variant Delta to
- 595 antibody neutralization. *Nature* 596, 276-280. 10.1038/s41586-021-03777-9.
- 596 41. Sterlin, D., Mathian, A., Miyara, M., Mohr, A., Anna, F., Claer, L., Quentric, P., Fadlallah, J., Devilliers, H.,
- 597 Ghillani, P., Gunn, C., et al. (2021). IgA dominates the early neutralizing antibody response to SARS-CoV-2.
- 598 *Sci Transl Med* 13. 10.1126/scitranslmed.abd2223.

599

600

601        **Acknowledgments**

602        The authors are grateful to Dr. Marie José Quentin-Millet and Estelle Besson (TheraVectys) for  
603 precious discussion and advices, to Magali Tichit et Sabine Maurin for excellent technical  
604 assistance in preparing histological sections, to Sébastien Chardenoux for excellent technical  
605 assistance in B6.K18-hACE2<sup>IP-THV</sup> mouse transgenesis, to Marie Laure Loriquet and Dr. Paul-Henri  
606 Consigny (Institut Pasteur Medical Center) for their gift of the leftover Moderna vaccines, not  
607 unusable in humans in a way that this study did not deprive any individual of a vaccine dose during  
608 the COVID-19 pandemic. The SARS-CoV2 variant Delta/2021/I7.2 200 was supplied by the Virus  
609 and Immunity Unit (Institut Pasteur, Paris, France) headed by Olivier Schwartz. The SARS-CoV-2  
610 Omicron BA.1 variant was initially supplied by the Virus and Immunity Unit (Institut Pasteur,  
611 Paris, France) headed by Olivier Schwartz, and was provided to our lab by Matthieu Prot and  
612 Etienne Simon-Lorière (G5 Evolutionary Genomics of RNA Viruses, Institut Pasteur, Paris,  
613 France).

614        This work was supported by TheraVectys and Institut Pasteur.

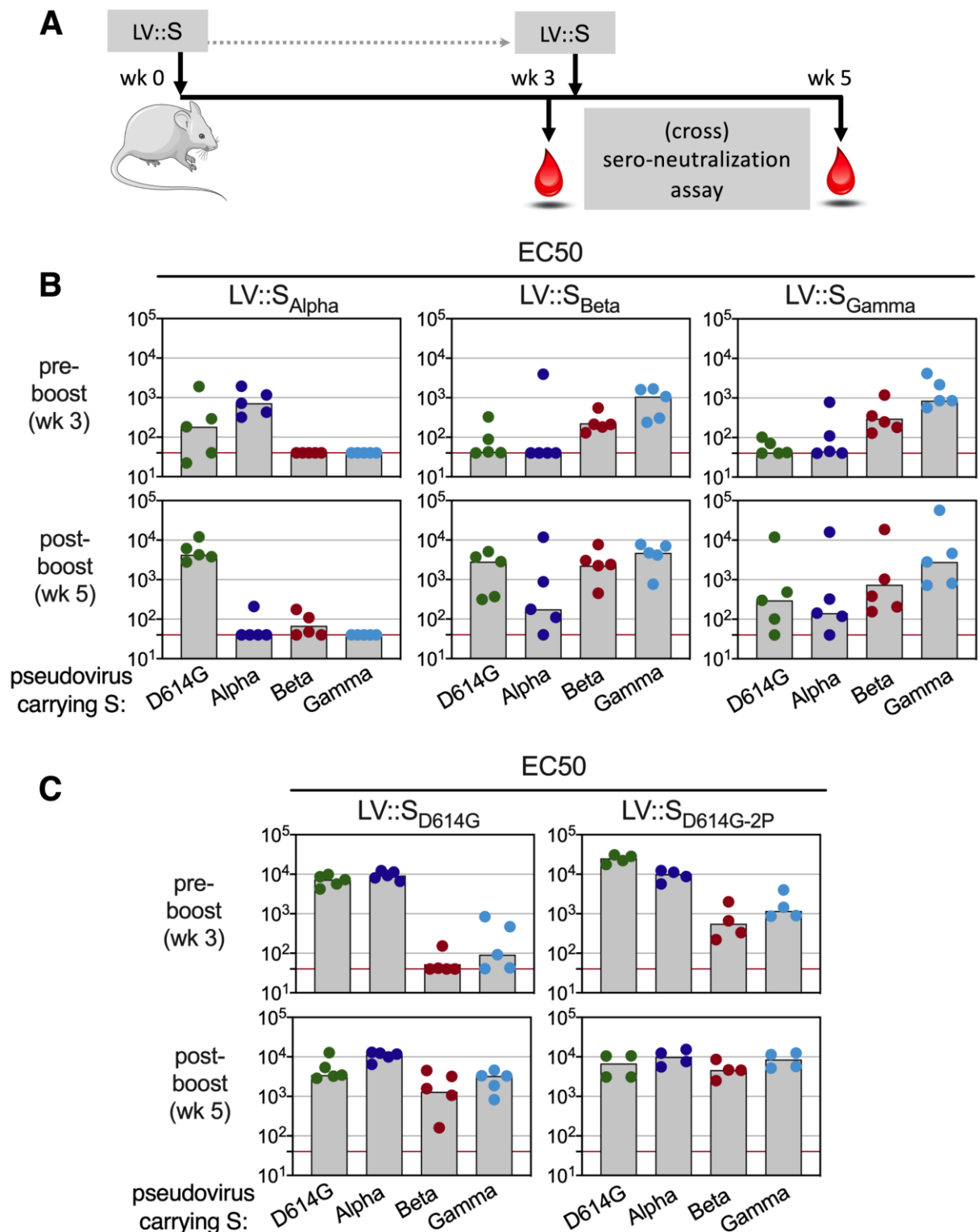
615        **Author Contributions**

616        Study concept and design: BV, JL, CG, MB, LM, PC, acquisition of data: BV, JL, AN, PA, IF,  
617 FLC, FM, KN, MB, LM, construction and production of LV and technical support: AN, FM, CB,  
618 FA, histology: FG, DH, recombinant Spike protein: CP, HM, collaborative generation of B6.K18-  
619 hACE2<sup>IP-THV</sup> transgenic mice: FLV, analysis and interpretation of data: BV, JL, FA, MB, LM, PC,  
620 drafting of the manuscript: LM.

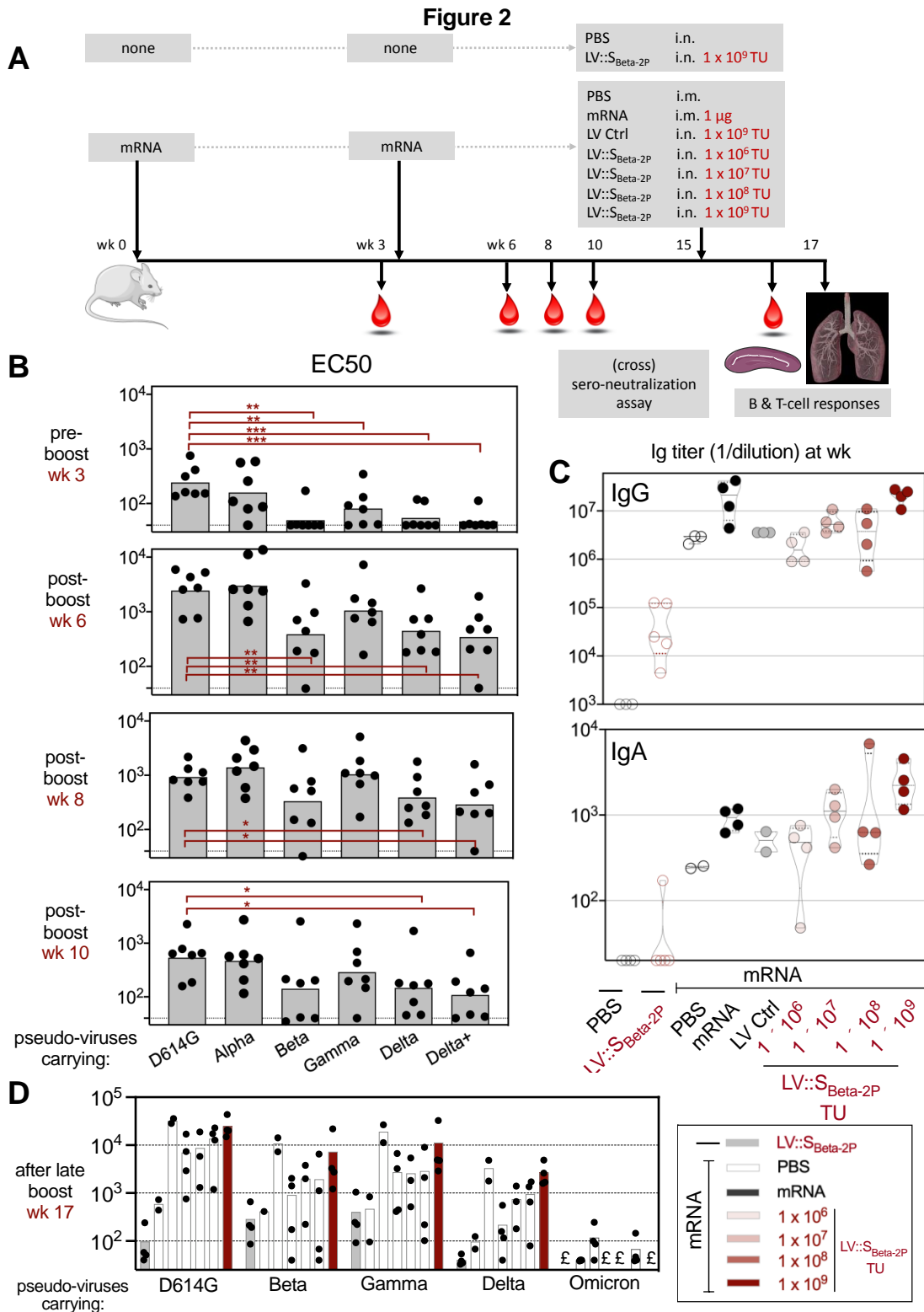
621        **Conflict of Interests**

622        PC is the founder and CSO of TheraVectys. BV, AN, PA, IF, FLC, FM, KN and FA are  
623 employees of TheraVectys. LM has a consultancy activity for TheraVectys. Other authors declare  
624 no competing interests. PA, IF, JL, BV, FA, MB, LM and PC are inventors of pending patents  
625 directed to the potential of i.n. LV::S vaccination against SARS-CoV-2.

Figure 1



626  
 627 **Figure 1. Down-selection of a S<sub>CoV-2</sub> variant with the highest potential to induce cross sero-**  
 628 **neutralizing antibodies. (A)** Timeline of prime-boost vaccination with LV::S<sub>Alpha</sub>, LV::S<sub>Beta</sub> or  
 629 LV::S<sub>Gamma</sub> and (cross) sero-neutralization assays in C57BL/6 mice ( $n = 4-5$ /group). **(B)** EC<sub>50</sub> of  
 630 neutralizing activity of sera from vaccinated mice was evaluated before and after the boost, against  
 631 pseudo-viruses carrying S<sub>CoV-2</sub> from D614G, Alpha, Beta or Gamma variants. **(C)** EC<sub>50</sub> of sera from  
 632 C57BL/6 mice, vaccinated following the regimen detailed in (A) with LV encoding for S<sub>D614G</sub>,  
 633 either WT or carrying the K<sup>986</sup>P - V<sup>987</sup>P substitutions in the S2 domain. EC<sub>50</sub> was evaluated before  
 634 and after the boost, as indicated in (B).



635

636

637

638

639

640

641

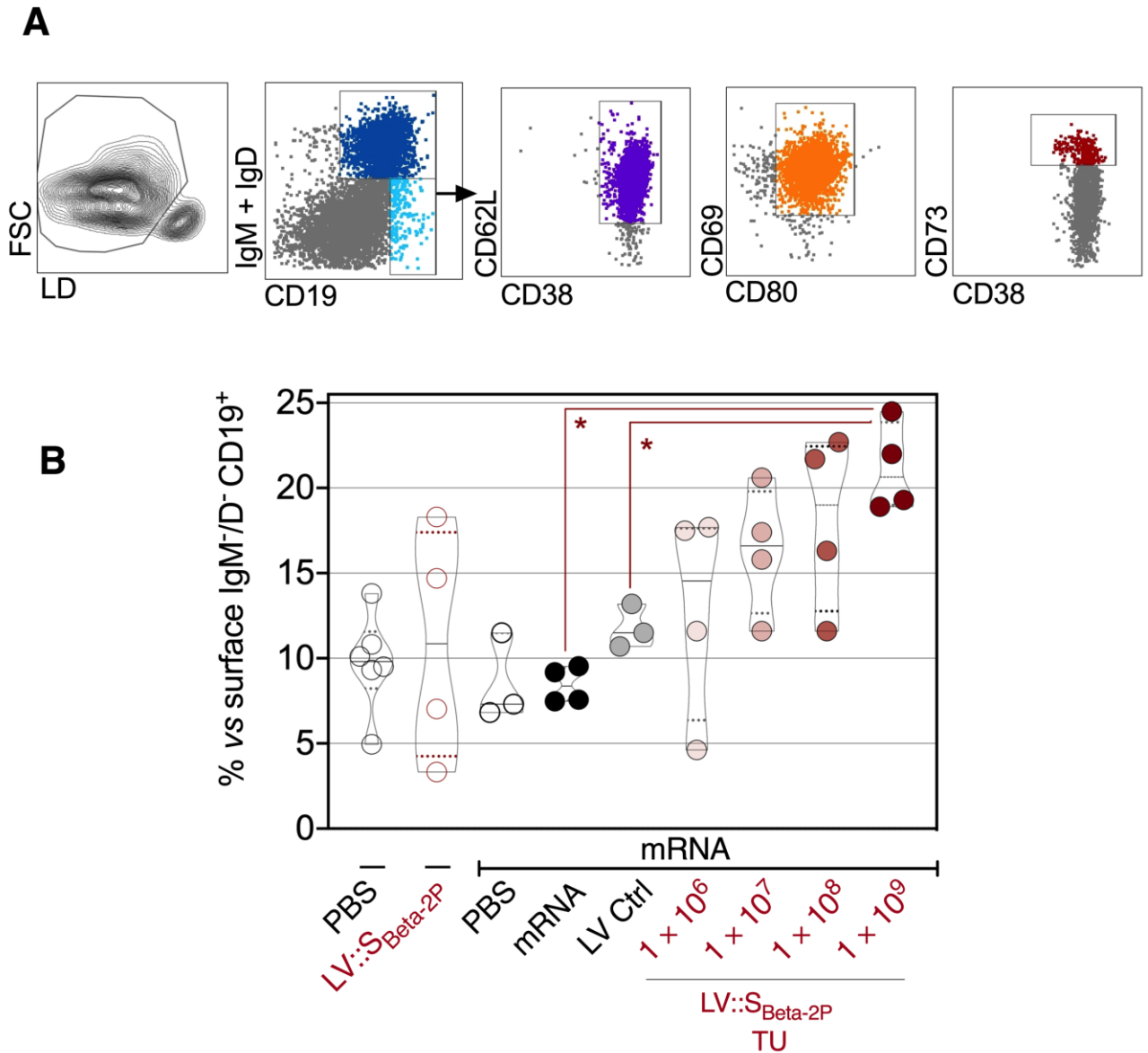
642

643

644

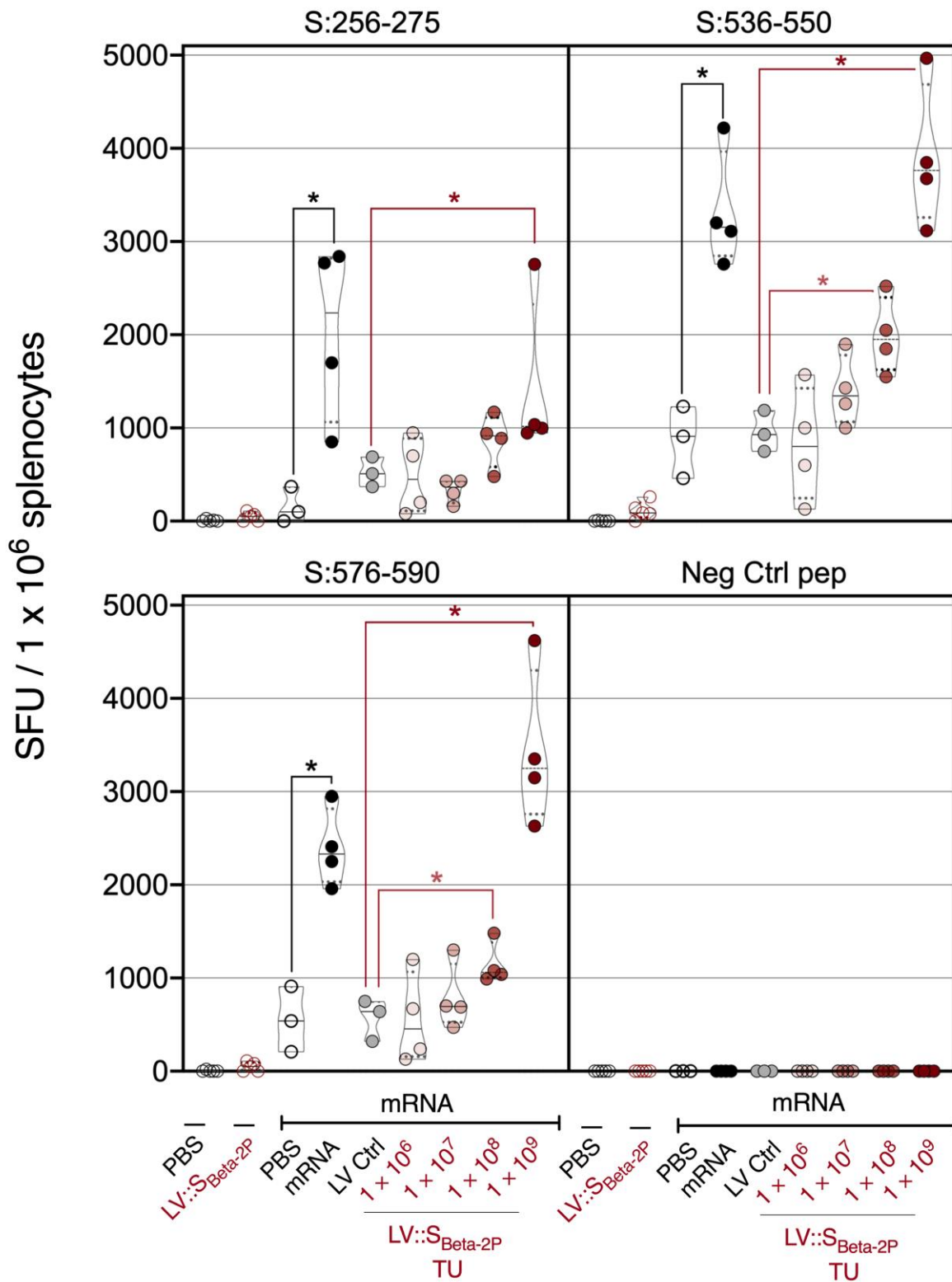
**Figure 2. Anti-S<sub>CoV-2</sub> humoral responses in mRNA-vaccinated mice which were further intranasally boosted with LV::S<sub>Beta-2P</sub>** (A) Timeline of mRNA i.m.-i.m. prime-boost vaccination in C57BL/6 mice which were later immunized i.n. by escalating doses of LV::S<sub>Beta-2P</sub> ( $n = 4-5/\text{group}$ ) and the (cross) sero-neutralization follow-up. (B) Serum EC50 determined at the indicated time points against pseudo-viruses carrying S<sub>CoV-2</sub> from D614G, Alpha, Beta, Gamma, Delta or Delta+ variants. (C) Anti-S<sub>CoV-2</sub> IgG (upper panel) or IgA (lower panel) titers in the sera two weeks after i.n. LV::S<sub>Beta-2P</sub> boost. Statistical significance was determined by Mann-Whitney test (\*=  $p < 0.05$ , \*\*=  $p < 0.01$ , \*\*\*=  $p < 0.001$ ). (D) Sera EC50, after the late boost given at wk 15, and as determined at wk 17. £ = not determined.

Figure 3



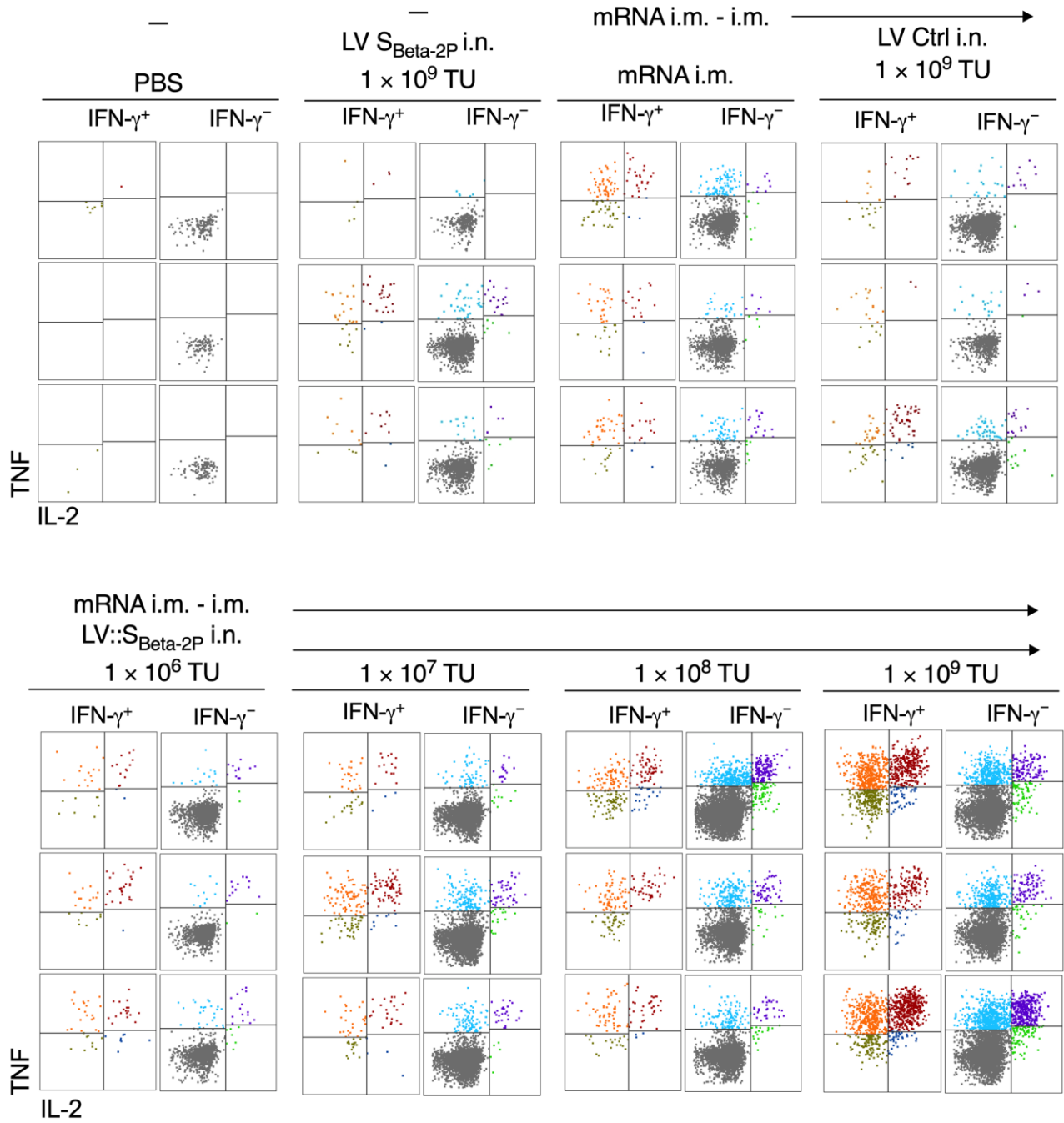
645  
646 **Figure 3. Lung B-cell resident memory subset in mRNA-vaccinated mice which were further**  
647 **intranasally boosted with LV::S<sub>Beta-2P</sub>.** The mice are those detailed in the Figure 2. Mucosal  
648 immune cells were studied two weeks after LV::S<sub>Beta-2P</sub> i.n. boost. (A) Cytometric gating strategy to  
649 detect lung Brm in mRNA-vaccinated mice which were further intranasally boosted with LV::S<sub>Beta-</sub>  
650 <sub>2P</sub>. (B) Percentages of these cells among lung CD19<sup>+</sup> surface IgM<sup>-</sup>/IgD<sup>-</sup> B cells in mRNA-  
651 vaccinated mice which were further intranasally boosted with LV::S<sub>Beta-2P</sub>. Statistical significance  
652 was determined by Mann-Whitney test (\*=  $p < 0.05$ ).  
653

Figure 4



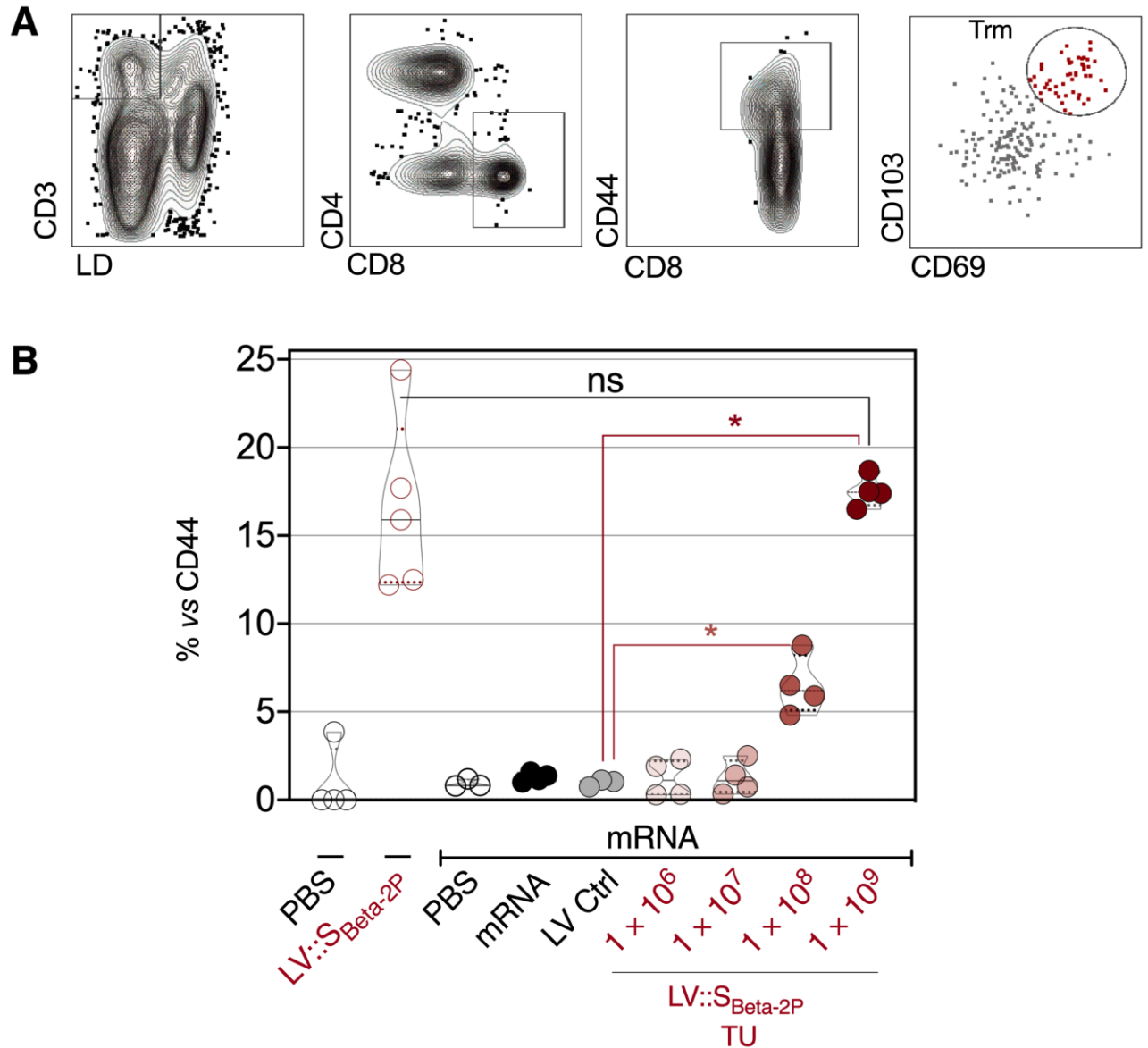
654  
 655 **Figure 4. Systemic CD8<sup>+</sup> T-cell responses to S<sub>CoV-2</sub> in mRNA-vaccinated mice which were**  
 656 **further intranasally boosted with LV::S<sub>Beta-2P</sub>.** The mice are those detailed in the Figure 2. T-  
 657 splenocyte responses were evaluated two weeks after LV::S<sub>Beta-2P</sub> i.n. boost by IFN- $\gamma$  ELISPOT  
 658 after stimulation with S:256-275, S:536-550 or S:576-590 synthetic 15-mer peptides encompassing  
 659 S<sub>CoV-2</sub> MHC-I-restricted epitopes. Statistical significance was evaluated by Mann-Whitney test (\*=  $p$   
 660 < 0.05).  
 661

**Figure 5**

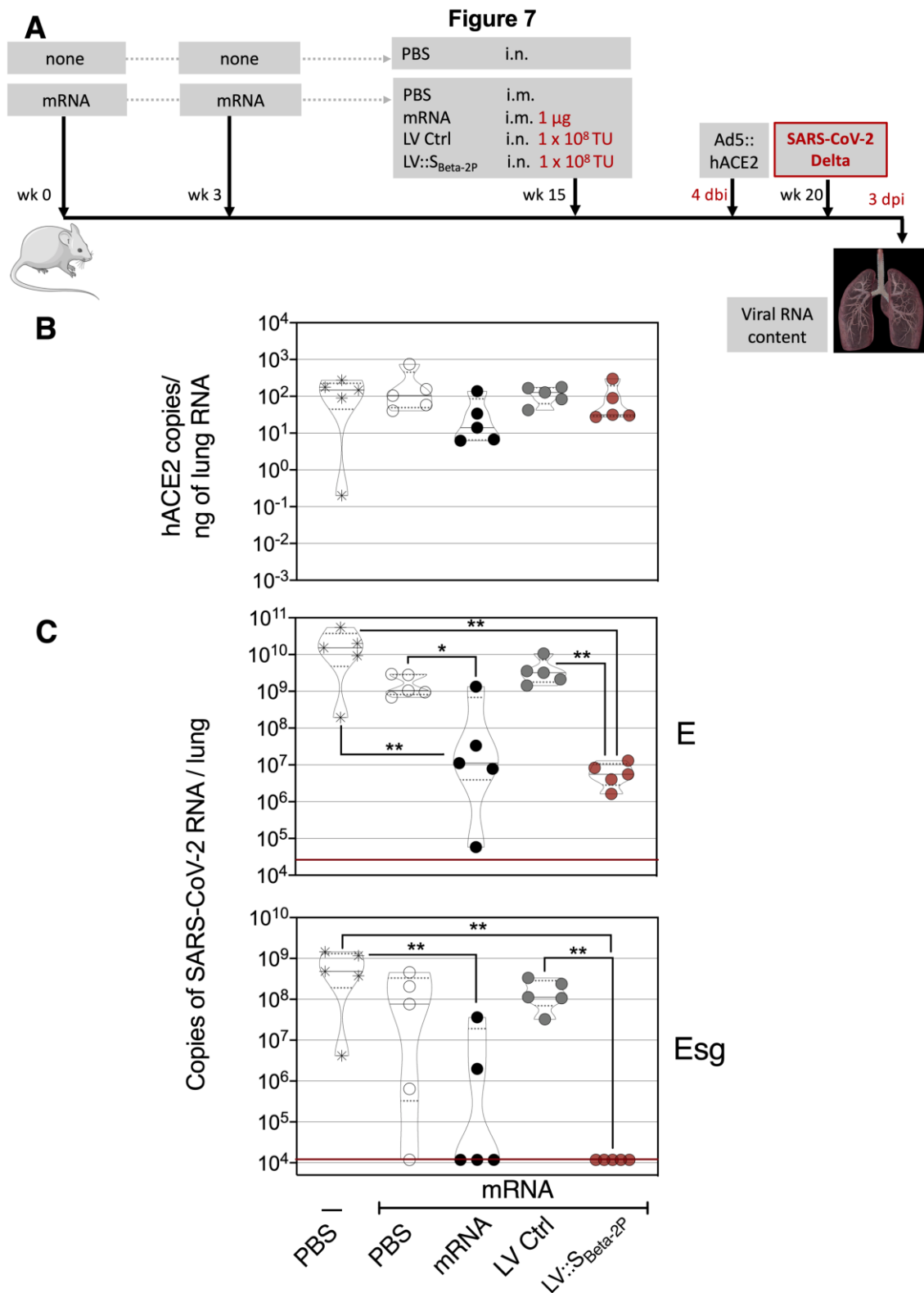


662  
 663 **Figure 5. Mucosal CD8<sup>+</sup> T-cell responses to S<sub>COV-2</sub> in mRNA-vaccinated mice which were**  
 664 **further intranasally boosted with LV::S<sub>Beta-2P</sub>.** The mice are those detailed in the Figure 2. (A)  
 665 Representative IFN- $\gamma$  response by lung CD8<sup>+</sup> T cells detected by intracellular cytokine staining  
 666 after in vitro stimulation with a pool of S:256-275, S:536-550 and S:576-590 peptides. Cells are  
 667 gated on alive CD45<sup>+</sup> CD8<sup>+</sup> T cells.  
 668

Figure 6



669  
 670 **Figure 6. Lung T resident memory subset in mRNA-vaccinated mice which were further**  
 671 **intranasally boosted with LV::S<sub>Beta-2P</sub>.** The mice are those detailed in the Figure 2. Mucosal  
 672 immune cells were studied two weeks after LV::S<sub>Beta-2P</sub> i.n. boost. **(A)** Cytometric gating strategy to  
 673 detect lung CD8<sup>+</sup> T resident memory (CD44<sup>+</sup>CD69<sup>+</sup>CD103<sup>+</sup>), and **(B)** percentages of this subset  
 674 among CD8<sup>+</sup> CD44<sup>+</sup> T-cells in mRNA-vaccinated mice which were further intranasally boosted  
 675 with LV::S<sub>Beta-2P</sub>. Statistical significance was evaluated by Mann-Whitney test (\*= *p* < 0.05).  
 676



677

678 **Figure 7. Full protective capacity of LV::S<sub>Beta-2P</sub> i.n. boost against Delta variant in initially**  
 679 **mRNA-primed and boosted mice. (A)** Timeline of mRNA i.m.-i.m. prime-boost vaccination in  
 680 C57BL/6 mice which were later immunized i.n. with  $1 \times 10^8$  TU/mouse of LV::S<sub>Beta-2P</sub> ( $n = 4-$   
 681  $5/\text{group}$ ), pre-treated i.n. with Ad5::hACE-2 4 days before i.n. challenge with  $0.3 \times 10^5$  TCID<sub>50</sub> of  
 682 SARS-CoV-2 Delta variant. **(B)** Comparative quantification of *hACE-2* mRNA in the lungs of  
 683 Ad5::hACE-2 pre-treated mice at 3 dpi. **(C)** Lung viral RNA contents, evaluated by conventional E-  
 684 specific (top) or sub-genomic Esg-specific (bottom) qRT-PCR at 3 dpi. Red lines indicate the  
 685 detection limits. Statistical significance was evaluated by Mann-Whitney test (\*=  $p < 0.05$ , \*\*=  $p <$   
 686  $0.01$ ).

